Electric Vehicle Traction Motor with a Reluctance Outer Rotor and a Modular Stator with AC Concentrated Toroidal Windings and PM or DC Wave Winding Excitation

Oluwaseun A. Badewa, Ali Mohammadi, Dan M. Ionel,
Somasundaram Essakiappan[1], and Madhav Manjrekar[1]
SPARK Laboratory, Stanley and Karen Pigman College of Engineering, University of Kentucky, Lexington, KY, USA
[1]QM Power, Inc., Kansas City, MO, USA
o.badewa@uky.edu, alimohammadi@uky.edu, dan.ionel@ieee.org,
somasundaram@qmpower.com, mmanjrekar@qmpower.com

***Abstract*—This paper proposes a novel electric motor concept using stator-embedded phase windings and can employ permanent magnet (PM) or Direct Current (DC) excitation. Concentrated toroidal coils are used for the phase windings and uniquely placed in separate slots while high flux intensification is achieved through a spoke-type arrangement of PMs or by using a DC excitation winding placed circumferentially around the stator. Torque production mechanism conforms with analytical concepts of air-gap flux density distributions using PM or DC excitation. High electrical loading can be achieved using DC excitation resulting in high power density as well as an extended power range through flux weakening by excitation current within thermal constraints. A comparison between this novel design and existing PM design previously analyzed and prototyped is carried out. Parametric studies as well as large scale multi-objective optimizations are used to find geometrical designs with best performance in terms of torque, total losses, torque ripple as well as power factor. Performance metrics such as power density, and machine goodness are used to compare this novel design with a ferrite design. The proposed novel design considers a 10″ outer rotor diameter with a torque of 550Nm at a base speed of 3,000rpm.**

***Index Terms*—Electric machines, synchronous motor, hybrid stator excitation, magnet-free, flux switching motor, PM motor, concentrated windings, finite element analysis.**

I. Introduction

Electric vehicles (EVs) continue to gain increasing shares in the automotive industry due to ever-increasing energy challenges, environmental concerns and an active shift towards more sustainable means of urban transportation [1, 2]. In order to be competitive against conventional vehicles, electric motors used in EVs must achieve high power density and efficiency within volumetric, cost, weight as well as material availability constraints by leveraging on advances in power electronics, battery technology as well as manufacturing.

A high power density motor shown in Fig.1a previously investigated and prototyped employed flux intensification techniques using tangentially magnetized rare-earth permanent magnets (PMs) and a reluctance type inner rotor and has the capability of meeting the stringent power density requirement of 50kW/L when integrated with advanced winding techniques for high slot fill factor and additively manufactured coils capable of withstanding high current densities. It also had additional benefits of high-speed operation, compact winding structure, modularized stator design, extended constant power range and provided a basis for further research [3–5]. A design employing non-rare earth PMs as shown in Fig.1b was also investigated and employed flux intensification techniques for low remenance PMs in an outer rotor design achieving comparable goodness with commercially available rare-earth PM motors in a bid to provide an alternative to use of rare-earth PMs due to availability concerns [6–8]. Beyond availability concerns, the challenges associated with the use of PMs as a whole such as magnet damage, risks of demagnetization, rotor eccentricity, unbalanced magnetic pull are undeniable and have fueled the push for magnet-free electric motors for electric traction applications [9, 10].

Apart from PM synchronous [11, 12], synchronous rotor DC excited [13, 14], and induction motors [15], which represent the typical choices for current practical EV traction applications, special machines, such as those typically referred to as switched or flux reversal machines, are considered in research, e.g. [16–18]. These flux switching machines (FSM) claim improved efficiency, high power density, and reduced reliance on rare-earth materials, making them an attractive option for electric vehicles.

In this paper, a novel design is proposed in which a DC wave excitation winding replaces PM excitation in the stator of an outer rotor motor as shown in Figs.1c and 1d to avoid the challenges associated with PMs while delivering comparable

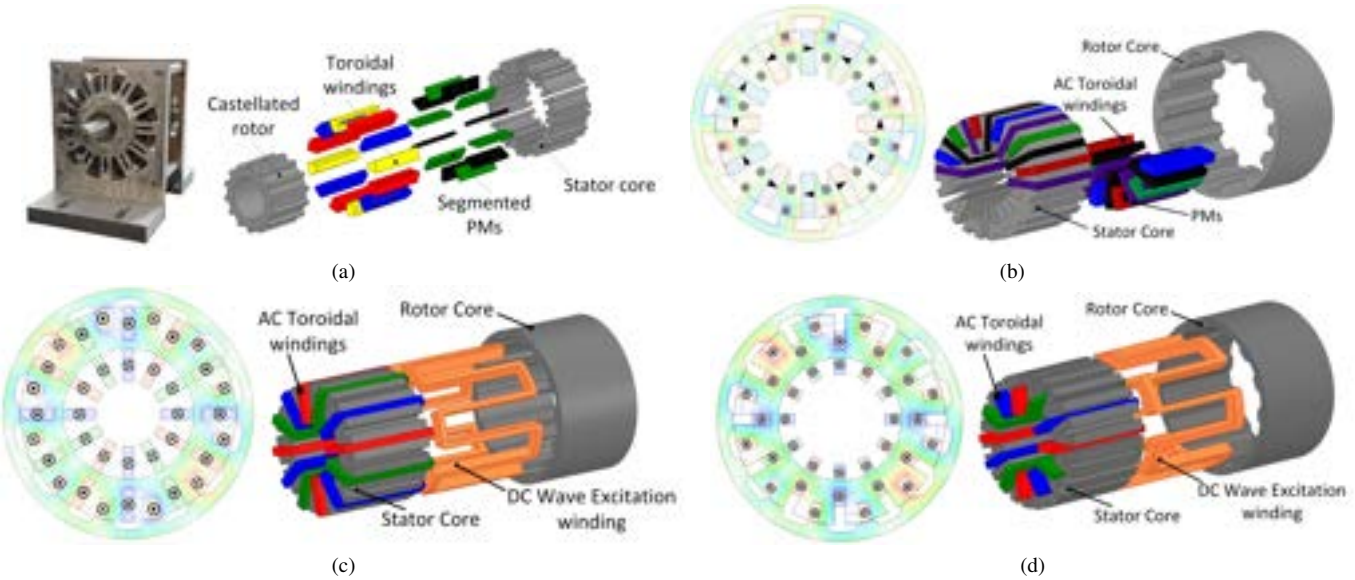

Fig. 1. Exploded and cross-sectional views of (a) high power density motor prototype using PM, (b) outer rotor design employing PM flux intensification techniques, (c) proposed novel design employing DC excitation with overlapping windings, and (d) proposed novel design employing DC excitation with non-overlapping windings. An alternative topology for the DC winding employs, similarly to the AC winding, concentrated toroidal coils and is not illustrated in the figure.

or better performance. The two designs show possibilities of overlap and non-overlap of the DC excitation winding with the AC windings providing flexibility in manufacturing.

II. Topology and Operation Principle of the Proposed Electric Motor

In previous works, flux intensification through the arrangement of toroidal windings as well as PM placements has been validated through electromagnetic simulations as well as from prototypes [3, 4, 19]. In the proposed topology, the PMs are replaced by one winding, which has the coil sides optimally placed in the stator core, and is supplied by a controlled DC voltage source to produce the excitation field in combination with the moving special reluctance consequent pole rotor as shown in Fig.1c [16, 20, 21].

The electromagnetic torque can then be obtained as:

$$T_{emg} = \frac{\partial}{\partial \theta_r} \int_V \frac{[B_{EX}(\phi,t) + B_{AR}(\phi,t)]^2}{2\mu_0} \mathrm{d}V, \qquad (1)$$

where $B_{EX}(\phi,t)$ and $B_{AR}(\phi,t)$ are on-load airgap flux density distributions of the DC excitation winding and armature windings respectively. The total magnetomotive force (MMF), F_{tot}, of the motor can also be expressed as:

$$F_{tot} = N_{ar} I_{ar} + N_{ex} I_{ex}, \qquad (2)$$

where N_{ar} and N_{ex} are the number of turns in the armature and excitation windings respectively, and I_{ar} and I_{ex} are the rms values of armature and field excitation currents respectively. Under ideal conditions and in the absence of saturation, for a fixed total MMF, maximum output for the proposed motor is obtained when the armature and excitation components are equal.

This novel design plays to several strengths such as the ready availability of copper as compared to rare-earth PMs, the deliberate use of rectangular slots to adopt the hairpin winding technology for high slot fill factor (SFF). Higher electrical loading can be applied to the DC wave excitation winding within acceptable thermal limits without fear of demagnetization, this implies the design is capable of wider constant power range as well as a greater degree of freedom as torque angle, AC supply, and DC excitation can all be controlled independently and these are valuable for flux weakening [16]. Also, the rotor is only made of laminated steel without any form of excitation making it suitable for very high speed operation. The stator can be modularized, fed with multiple inverters, and effectively cooled from within due to the exposed AC windings thereby improving performance and reliability.

III. Design Considerations and Multi-Objective Optimization

Preliminary parametric studies carried out have shown that between a choice of 10 and 14 protrusions for the rotor, 14 protrusions yield higher torque, efficiency, and power density and has therefore being selected for this topology [3, 22, 23]. By defining a slot depth to pole pitch ratio ζ given as:

$$\zeta = \frac{4h_{ex}}{\tau_s}, \qquad (3)$$

where h_{ex} is the depth of slot for DC coils along the rotor radius, and τ_s is the stator pole pitch, i.e., stator outer circumference πD_s divided by the number of excitation coil sides n_{ex}, performance metrics such as the average airgap flux density B_{avg}, excitation index E_{ind}, and machine goodness GD can be studied using 2D FEA on Ansys Electronics

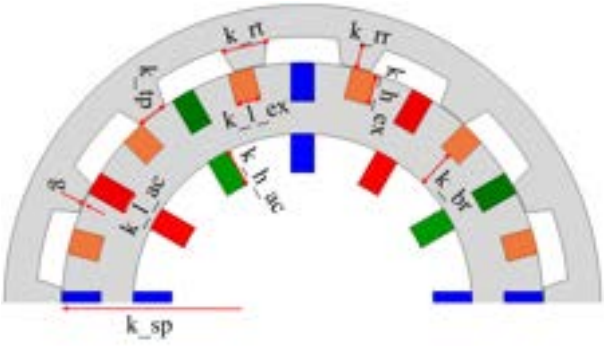

(a)

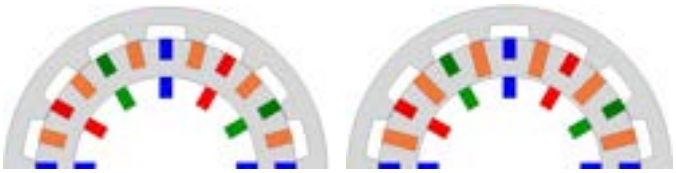

(b) (c)

Fig. 2. Models of proposed motor design considering different slot depth to pole pitch ratios of (a) 1.0, (b) 1.5, and (c) 2.0.

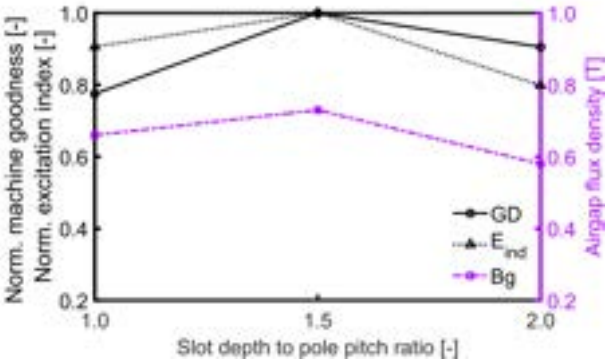

Fig. 3. Machine goodness, excitation goodness, and absolute average airgap flux density at open-circuit for different slot depth to pole pitch ratios.

software [5] to see the effect of winding side depth on motor performance. The excitation index E_{ind} is defined as:

$$E_{ind} = \frac{h_{ex} B_{avg} \ell_{stk}}{M_{ex}}, \tag{4}$$

where M_{ex} is the mass of one coil side of the excitation winding along the stack length, while the machine goodness GD is expressed as:

$$GD = \frac{T_{emg}}{\sqrt{W_{loss}}}, \tag{5}$$

where W_{loss} is the total motor loss. The total loss in this motor is comprised of components in the laminated core, and

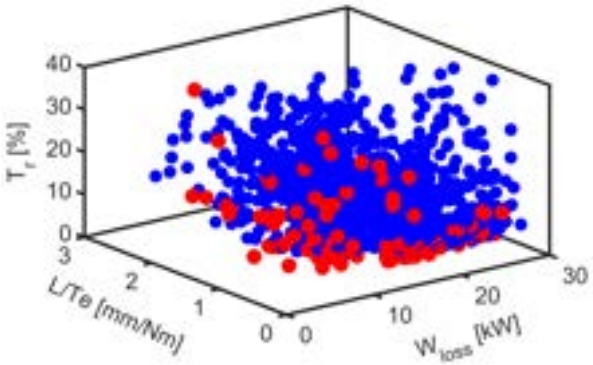

Fig. 4. Optimization results: 3D pareto front projection with objectives of stack length to average torque, total loss, and torque ripple.

winding copper, is calculated as:

$$\begin{aligned} W_{loss} &= W_{Cu} + W_{we} + W_{Fe} \\ &= 3R_{ph}I_{ph}^2 + R_{ex}I_{ex}^2 + W_{we} \\ &+ \sum \left[W_h\left(B, f\right) + W_e\left(B, f^2\right) \right], \end{aligned} \tag{6}$$

where R_{ph} and I_{ph} are the AC winding resistance and current per phase respectively, R_{ex} and I_{ex} are the DC excitation winding resistance and current respectively, and W_{we} the eddy current losses in the winding. Core losses include hysteresis W_h, and eddy current losses W_e, both as a function of frequency f, and magnetic flux density B. For the purpose of this study, W_{we} have been considered negligible. Slot depth to pole pitch ratios ζ of 1.0, 1.5, and 2.0 are investigated as shown in Fig.3. The results indicate that out of the three ratios, a ratio of 1.5 gives the best results with a B_{avg} of 0.73T, E_{ind} of 5.76Wb/kg and GD of 3.6Nm/sqrt(W) and is considered an optimal choice for this motor topology.

Multi-objective optimization employing differential evolution (DE) and FEA was carried out to minimize three concurrent objectives relating to the ratio of stack length to average torque $\mathcal{F}_1$, total power loss $\mathcal{F}_2$, and torque ripple $\mathcal{F}_3$:

$$\begin{aligned} \mathcal{F}_1 &= \frac{\ell_{stk}}{T_{avg}}, \\ \mathcal{F}_2 &= W_{loss} = W_{Cu} + W_{Fe}, \\ \mathcal{F}_3 &= T_r = \frac{T_{\max} - T_{\min}}{T_{avg}} \times 100\%, \end{aligned} \tag{7}$$

with an additional *constraint* on the power factor to a minimum value of 0.7. Independent variables that control the motor geometry as shown in Fig. 2a, and their ranges for the optimization were selected based on parametric studies to ensure a wide optimization area and production of robust and mechanically stable designs.

IV. Results and Discussion

The 3D Pareto of the optimization results shows that the best designs represented by red dots have the lowest values of

Table I
PERFORMANCE COMPARISON OF A REFERENCE DESIGN WITH FERRITE AND PROPOSED NOVEL DESIGN EMPLOYING DC EXCITATION

Ref.	Peak torque [Nm]	T_r [%]	K_T [Nm/A/mm^2]	Goodness [Nm/$\sqrt{W_{loss}}$]	Active Mass [kg]	Power Density [kW/L]	Power Density [kW/kg]
OR-PM	373	10	12.4	3.7	38	13.2	3.1
OR-DC D1	526	3	17.5	3.2	41	22.8	4.1
OR-DC D2	593	18	19.8	3.9	41	25.5	4.6

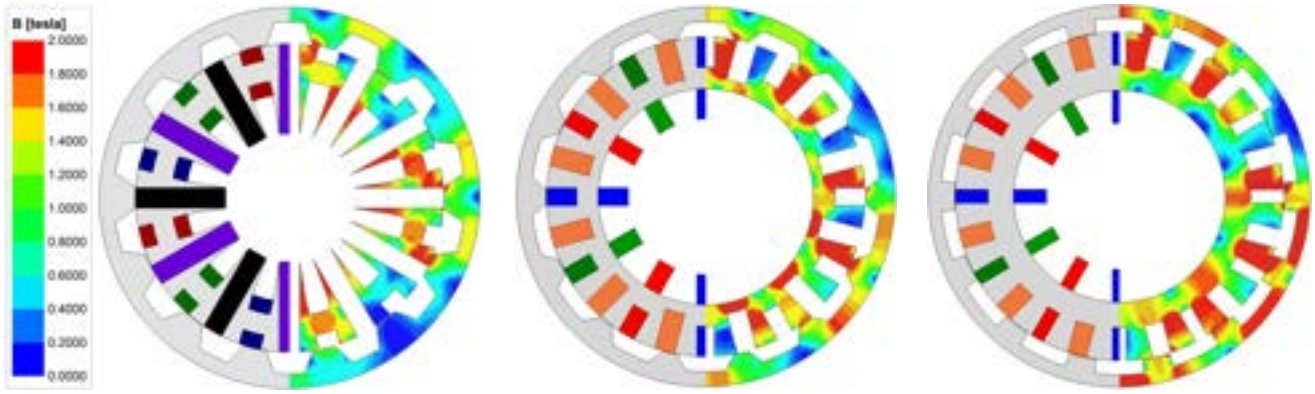

(a) (b) (c)

Fig. 5. Cross-sectional view with flux density and lines at high electrical loading of 30A/mm^2 for (a) Outer rotor design with 0.4T remenance ferrite "OR-PM", (b) optimization "best" design-1 outer rotor design with DC excitation "OR-DC D1" and, (c) optimization "best" design-2 outer rotor design with DC excitation "OR-DC D2".

Table II
PERFORMANCE SPECIFICATIONS FOR OR-DC D2

Parameter	Value	Unit
Peak torque	593	Nm
Continuous torque	241	Nm
Max. power	186	kW
Base speed	3,000	rpm
Max. speed	14,400	rpm
Emag eff. at peak torque	89	%
Emag eff. at continuous torque	94	%
Rotor OD	255	mm
Stack length	150	mm
Total active mass	41	kg

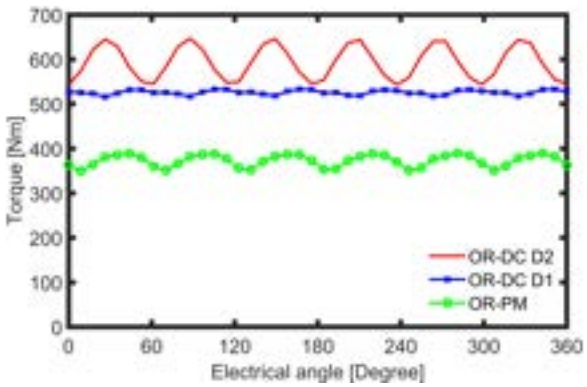

Fig. 6. Torque waveform for OR-PM, OR-DC D1, and OR-DC D2 designs.

stack length to average torque, torque ripple and total losses as shown in Fig.4. Comparison of cross-sections as well as torque waveforms of selected "best" designs to previously investigated PM design is as in Figs. 5 and 6 respectively at anticipated high electrical loading of 30A/mm^2 owing to the integration of advanced cooling techniques and zero risk of demagnetisation in the DC-excited design. This machine may also benefit from the use of superconducting materials in the excitation winding availing the opportunity for even higher current densities and increased power density [24].

The DC-excited designs OR-DC D1 and D2 are seen to have comparable goodness with OR-PM while achieving higher torque and power density within the same volume as the ferrite design as shown in Table I. Low torque ripple operation is possible as shown in OR-DC D1 with a trade off in torque when compared with D2. A summary of the performance specifications for the selected "best" design OR-DC D2 is given in table II.

A comparison of the selected "best" designs with commercially available high power density traction motors considering their approximate performances based on publicly available information is as given in Table III. Analysed designs shows competitive performance with these commercially available state-of-art motors [25].

The flux weakening ability of the proposed design by varying the combinations of AC current density J_{ac}, and DC excitation current density J_{dc} at a given torque angle and speed is as shown in Fig.7. Due to the multiple degrees of freedom available for the operation of the proposed motor,

Table III
PERFORMANCE COMPARISON WITH HIGH POWER DENSITY TRACTION MOTORS

	Type	Peak Te [Nm]	Active Mass [kg]	TRW [Nm/kg]
OR-PM	New	373	38	9.8
OR-DC D1	New	526	41	12.8
OR-DC D2	New	593	41	14.5
Honda Accord 14	IPM (V)	306	33	9.3
YASA 400	Axial PM	360	24	15.0
Toyota Prius 10	IPM (V)	207	23	9.0
Chevrolet Bolt EV	IPM (V)	360	33	10.9
Tesla S	Induction	430	55	7.8

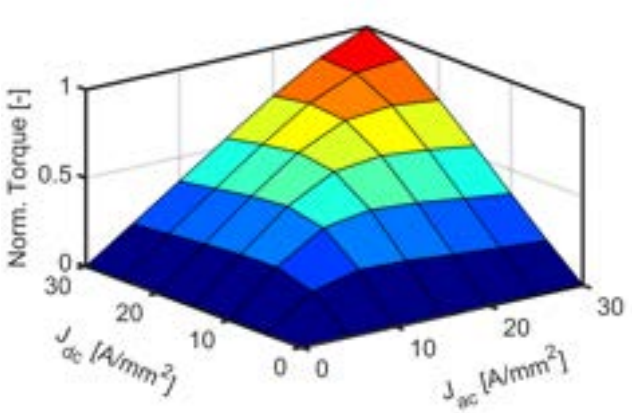

Fig. 7. Control characteristics for proposed motor design through AC supply, and DC excitation control.

several control strategies can be applied.

V. CONCLUSION

A special outer-rotor electric machine topology was proposed, simulated, and optimized for electric vehicle traction applications. In the proposed design, possibilities exist for the use of DC as well as PM excitation. The outer rotor design eliminates the mechanical limitations imposed by an outer stator design allowing for a geometrically larger rotor and increased effective winding area resulting in greater average torque and power density values. Rectangular slots in design are adapted for hairpin winding technology and highly efficient cooling arrangements can also be employed in the proposed design due to losses being localized in stator only as well as AC windings placement with exposed sides.

In the analysed design focusing on the use of DC excitation, it has been shown that the challenges associated with PMs can be eliminated while achieving comparable machine goodness, higher torque, and power density. A comparison of the proposed motors with state-of-the art high power density traction motors shows competitive performance in terms of torque per weight as well as active mass.

Extended power ranges and high power density may be achieved in this motor topology with zero risk of demagnetisation through higher electrical loading enabled by integrated advanced cooling techniques. The motor topology also has several degrees of freedom in its operation and can benefit from different control strategies.

ACKNOWLEDGMENT

The support of QM Power, Inc., Ansys Inc., and University of Kentucky the L. Stanley Pigman Chair in Power endowment is gratefully acknowledged.

REFERENCES

[1] B. Sarlioglu, C. T. Morris, D. Han, and S. Li, "Driving toward accessibility: a review of technological improvements for electric machines, power electronics, and batteries for electric and hybrid vehicles," *IEEE Industry Applications Magazine*, vol. 23, no. 1, pp. 14–25, 2016.

[2] I. Husain, B. Ozpineci, M. S. Islam, E. Gurpinar, G.-J. Su, W. Yu, S. Chowdhury, L. Xue, D. Rahman, and R. Sahu, "Electric drive technology trends, challenges, and opportunities for future electric vehicles," *Proceedings of the IEEE*, vol. 109, no. 6, pp. 1039–1059, 2021.

[3] P. Han, M. G. Kesgin, D. M. Ionel, R. Gosalia, N. Shah, C. J. Flynn, C. S. Goli, S. Essakiappan, and M. Manjrekar, "Design optimization of a very high power density motor with a reluctance rotor and a modular stator having PMs and toroidal windings," in *2021 IEEE Energy Conversion Congress and Exposition (ECCE)*. IEEE, 2021, pp. 4424–4430.

[4] M. Rosu, P. Zhou, D. Lin, D. M. Ionel, M. Popescu, F. Blaabjerg, V. Rallabandi, and D. Staton, *Multiphysics simulation by design for electrical machines, power electronics and drives*. John Wiley & Sons, 2017.

[5] *Ansys® Electronics, Maxwell, version 23.1, 2023, ANSYS Inc.*

[6] O. A. Badewa, A. Mohammadi, D. D. Lewis, D. M. Ionel, S. Essakiappan, and M. Manjrekar, "Optimization of an electric vehicle traction motor with a PM flux intensifying stator and a reluctance outer rotor," in *2023 IEEE Transportation Electrification Conference & Expo (ITEC)*, 2023.

[7] M. Obata, S. Morimoto, M. Sanada, and Y. Inoue, "Performance of PMASynRM with ferrite magnets for EV/HEV applications considering productivity," *IEEE Transactions on Industry Applications*, vol. 50, no. 4, pp. 2427–2435, 2014.

[8] D. Wang, W. Feng, B. Wang, G. Xu, and X. Wang, "Design, prototype and experimental verification of single phase flux switching motor using low cost magnets," *IEEE Transactions on Energy Conversion*, vol. 38, no. 1, pp. 284–295, 2023.

[9] S. Choi, M. S. Haque, M. T. B. Tarek, V. Mulpuri, Y. Duan, S. Das, V. Garg, D. M. Ionel, M. A. Masrur, B. Mirafzal *et al.*, "Fault diagnosis techniques for permanent magnet AC machine and drives—a review of current state of the art," *IEEE Transactions on Transportation Electrification*, vol. 4, no. 2, pp. 444–463, 2018.

[10] A. Mohammadi, Y. Chulaee, C. Aaron, I. Boldea, and D. M. Ionel, "Axial flux permanent magnet vernier machine with single-wound dual-stator and spoke permanent magnet rotor for electric vehicle in-wheel traction," in *2023 IEEE Transportation Electrification Conference & Expo (ITEC)*, 2023.

[11] L. Parsa and H. A. Toliyat, "Fault-tolerant interior-permanent-magnet machines for hybrid electric vehicle applications," *IEEE Transactions on Vehicular Technology*, vol. 56, no. 4, pp. 1546–1552, 2007.

[12] S. Cai, Z. Zhu, L. Huang, and H. Qu, "Comparison of stator slot permanent magnet hybrid excited machine with rotor interior permanent magnet machine for EV/HEV application," in *The*

10th International Conference on Power Electronics, Machines and Drives (PEMD 2020), vol. 2020, 2020, pp. 645–650.

[13] I. Boldea, L. N. Tutelea, L. Parsa, and D. Dorrell, "Automotive electric propulsion systems with reduced or no permanent magnets: An overview," *IEEE Transactions on Industrial Electronics*, vol. 61, no. 10, pp. 5696–5711, 2014.

[14] S. Jia, R. Qu, J. Li, and Y. Chen, "Comparison of stator DC-excited vernier reluctance machines with synchronous reluctance machines," in *2015 IEEE International Electric Machines Drives Conference (IEMDC)*, 2015, pp. 649–655.

[15] J. Mei, Y. Zuo, C. H. T. Lee, and J. L. Kirtley, "Modeling and optimizing method for axial flux induction motor of electric vehicles," *IEEE Transactions on Vehicular Technology*, vol. 69, no. 11, pp. 12 822–12 831, 2020.

[16] Y. Tang, J. Paulides, T. Motoasca, and E. Lomonova, "Flux-switching machine with DC excitation," *IEEE Transactions on Magnetics*, vol. 48, no. 11, pp. 3583–3586, 2012.

[17] J. D. McFarland, T. M. Jahns, and A. M. EL-Refaie, "Analysis of the torque production mechanism for flux-switching permanent-magnet machines," *IEEE Transactions on Industry Applications*, vol. 51, no. 4, pp. 3041–3049, 2015.

[18] H. Chen, X. Liu, N. A. O. Demerdash, A. M. EL-Refaie, J. Zhao, and J. He, "Comparison and design optimization of a five-phase flux-switching PM machine for in-wheel traction applications," *IEEE Transactions on Energy Conversion*, vol. 34, no. 4, pp. 1805–1817, 2019.

[19] D. M. Ionel, J. Eastham, and T. Betzer, "Finite element analysis of a novel brushless DC motor with flux barriers," *IEEE Transactions on Magnetics*, vol. 31, no. 6, pp. 3749–3751, 1995.

[20] A. Mohammadi, O. A. Badewa, Y. Chulaee, D. M. Ionel, S. Essakiappan, and M. Manjrekar, "Direct-drive wind generator concept with non-rare-earth PM flux intensifying stator and reluctance outer rotor," in *2022 11th International Conference on Renewable Energy Research and Application (ICRERA)*, 2022, pp. 582–587.

[21] G. Heins, D. M. Ionel, and M. Thiele, "Winding factors and magnetic fields in permanent-magnet brushless machines with concentrated windings and modular stator cores," *IEEE Transactions on Industry Applications*, vol. 51, no. 4, pp. 2924–2932, 2015.

[22] S. M. Castano, R. Yang, C. Mak, B. Bilgin, and A. Emadi, "External-rotor switched reluctance motor for direct-drive home appliances," in *IECON 2018 - 44th Annual Conference of the IEEE Industrial Electronics Society*, 2018, pp. 514–521.

[23] B. Anvari, H. A. Toliyat, and B. Fahimi, "Simultaneous optimization of geometry and firing angles for in-wheel switched reluctance motor drive," *IEEE Transactions on Transportation Electrification*, vol. 4, no. 1, pp. 322–329, 2017.

[24] S. Saeidabadi, C. Kovacs, A. Usman, T. J. Haugan, K. Corzine, and L. Parsa, "Flux switching machines- for all-electric aircraft applications," in *2022 International Conference on Electrical Machines (ICEM)*, 2022, pp. 1430–1436.

[25] A. Fatemi, D. M. Ionel, M. Popescu, Y. C. Chong, and N. A. Demerdash, "Design optimization of a high torque density spoke-type PM motor for a formula E race drive cycle," *IEEE Transactions on Industry Applications*, vol. 54, no. 5, pp. 4343–4354, 2018.